

Effect of Inlet Swirl on Combustion Performance and Soot Formation of a Turbulent Methane-Air Non-Premixed Flame

Tarak Kumar Sahoo, Prakash Ghose*

School of Mechanical Engineering, KIIT Deemed to be University, Bhubaneswar-24, INDIA

Received 11 OCT 2021

Accepted 7 FEB 2022

Abstract

In the present study, the effect of swirl intensity on flame temperature, radiation heat flux, soot formation, dispersion, and other major species concentrations were investigated for methane-air non-premixed combustion. Harwell standard furnace has been chosen for computational modeling. Eddy dissipation combustion model is used to evaluate reaction rate considering one-step global combustion reaction mechanism for methane. Standard k- ϵ turbulent model, Discrete ordinate (DO) radiation model, and Moss-Brookes soot models are used for simulation. The weighted-sum-of-gray-gases model (WSGGM) is employed to calculate the radiation absorption coefficient. A fair agreement has been observed between published experimental and simulation results. The numerical results show that as the swirl intensity increases, the radial component of the flow increases, hence the flame becomes wider. Consequently, the temperature distribution, soot formation, and the species mass concentration are also strongly influenced by the swirl intensity. It has also been observed that the flame temperature decreases with the consideration of soot generation due to an increase in radiation heat loss of eight percent. Incomparable to any swirl, the average wall heat flux increases to 62.72% when the swirl number is 5.

© 2022 Jordan Journal of Mechanical and Industrial Engineering. All rights reserved

Keywords: Swirl number, Radiation heat flux, Soot formation, Species mass fraction.

1. Introduction

At present, a major part of the total energy across the globe depends on fossil fuels such as; coal, oil, and natural gas. Natural gas is primarily composed of methane which is mostly used as fuel for homes, kilns, automobiles, turbines, and other machinery. Methane combustion emits unburned hydrocarbons, carbon dioxide, oxides of nitrogen, etc.[1]. These emissions are exhausted into surroundings, pollute the atmosphere, and are responsible for climate change. To minimize fuel loss and pollution, researchers mainly focused on the finding of maximum combustion efficiency with minimum harmful emissions.

Emissions can be minimized with the complete combustion of fuel. To enhance the combustion efficiency, air feed into the combustion chamber through a swirler is a well-adapted methodology. Because of the swirling action of air, the unburnt fuel is pulled back into the flame region due to adverse pressure gradient, hence the combustion efficiency increases. The effect of swirl has been studied by many researchers both experimentally and numerically. Swirler is also called a flame holding device because it provides stability to the flame by minimizing the flame blowout possibility [2], [3]. Reverse flows are the reasons for the larger residence time of the air-fuel mixture to be present in the flame zone and enhanced combustion as well [4]. Swirl increases the turbulent intensity inside the combustor and thereby affects the scalar variable distribution. It also helps in stabilizing the complex turbulent flames[2]. Iyogun et al.[5] experimentally found that, with the increase in swirl number, a relatively larger recirculation zone is formed with a rectangular nozzle as

compared to a circular counterpart. Saediamiri et al.[6] investigated the effect of low swirl intensity of co-flow air and nozzle diameter on flame stability. It has been reported that swirl has a significant effect on moderate to high co-flow air velocity, but it is not much significant when co-flow air velocity is very less. Sellan et al.[7] implemented swirlers both in the outer and inner air stream where the inner airflow velocity is 2-3 times than the outer air stream. It has been observed that the combined arrangement of the swirler is more effective in flame holding rather than a single inner swirler. Yoon et al.[8] experimentally exhibited the effect of swirl intensity on the combustion and its emission characteristics. They found that by increasing the swirl intensity, the particulate matter and carbon monoxide emissions can be reduced, but the NO_x emissions will increase.

The formation of soot particles during combustion is one of the major environmental pollutions as it can damage the respiratory system of any living being. Soot emission is also a primary cause of global warming. Hence, proper prediction of soot in combustion through computational modeling is very much necessary. Ogawa et al.[9] investigated the effect of the swirl ratio on the NO_x and soot emissions with the help of the KIVA code. They found that relatively stronger swirl intensity reduces soot emissions up to an optimum limit and further increases in swirl intensity, soot emissions increase. Bonatesta et al.[10] have computationally investigated the soot in an internal combustion engine and found that, in the cylinder, the fuel distribution and the location of combustion are the most influential parameters for the soot formation. An increased

* Corresponding author e-mail: pghosefme@kiit.ac.in.

level of swirl intensity downgrades the combustion by increasing soot formations. Chong et al.[11] studied the combustion behavior of a model aircraft combustor, where a Large-eddy simulation modeling approach is used to incorporate the turbulent effects in the flow field. They found that a very high amount of soot formation occurs on and around the fuel jet. A small set of fuel trajectories deposition on the fuel jets is the prime reason for soot deposition in this part, and that happens due to the swirling action. Zhou et al.[12] experimentally studied the soot emissions in a separated swirl combustion system (SSCS) and compared with a double swirl combustion system (DSCS). They found SSCS produces less incipient soot particles than DSCS, and SSCS has a faster surface soot oxidation. The relationships between soot distribution, flame structure, and the flow field were experimentally investigated for diffusion flames of methane and air by Wang et al.[13]. They observed that the reduction in soot particles with airflow rate is correlated with high-intensity turbulence and elevated oxidation rate in the recirculation zone.

In numerical studies, Keramida et al.[14] used two different radiation models, such as the Discrete transfer model and the Six-flux model, to predict the effect of radiation models on combustion characteristics. They perceived the importance of the thermal radiation effect even in a low-temperature flame. However, to check the performance prediction of both the radiation model, simulated results were verified against the experimental work of Wilkes et al.[15]. Ghose et al.[16] numerically simulated a kerosene fuel spray combustor to speculate the soot formation and effects of thermal radiation at various swirl intensities. The Brookes and Moss[17] augmented soot model for kerosene flames which has been used to evaluate the radiant heat flux on the combustor wall and fuel injector. They found incident heat flux on the wall decreases as the swirl intensity is reduced. Moreover, a uniform temperature distribution in the exhaust gas is obtained in the combustor exit with higher swirl intensity. Yilmaz[18] used AnsysFluent code for numerical simulations of natural gas non-premixed combustion. He used the Eddy dissipation model with one step combustion reaction mechanism, Standard k-ε turbulence model for turbulent closure, and P-1 radiation model flame radiation inside the combustor to verify the effect of the swirl number on flame temperature and the gas concentrations such as CH₄, O₂, CO₂, and H₂O. He found the intensity of the swirl changes the fluid dynamics characteristics of a diffusion flame, such as axial velocity distribution, central recirculation zone, and the external circulation zone.

Yang et al.[19] used Harwell combustor model, and simulated the turbulence radiation interaction (TRI) to acknowledge the radiation characteristics with oxy-combustion conditions. They observed that it strongly affects the temperature fields. Moreover, with increasing the swirl intensity, the TRI effect decreased.

RANS (Reynolds average Navier-Stokes) equations are solved to simulate the turbulent flow. By time averaging of Navier-Stokes equations, RANS equations are derived. The additional terms during averaging of Navier-Stokes equation are evaluated from the Boussinesque hypothesis. RANS has a minimal computational need. Therefore, it is generally used in highly complex geometry where the mesh number is very high. Many researchers used RANS-based turbulent models (various k-ε models) [20][21] and observed that the flow variables are properly predicted by those models.

Seeing the vital role of swirling the combustor, and consequently, the combustion behaviors, it is obligatory to determine its accurate intensity for modeling combustion phenomena. In the light of the above discussions, the present study focuses on the effect of swirl on comprehensive combustion performance. The effect of various levels of swirl intensities on radiant heat flux and soot generation has been investigated; as it was rarely explored in previous articles. The existing experimental data are compared with similar computational and experimental results.

2. The details of models:

2.1. Combustor geometry and boundary conditions

In this paper, the Harwell furnace[15] has been chosen to investigate the swirling effect and the combustion characteristics of methane-air diffusion flame. The length and the radius of the combustion chamber are 900 mm and 150 mm respectively as shown in Figure-1. The air is supplied through the annular hole at a velocity of 12.8 m/s and the fuel is supplied through the central hole at a velocity of 0.15 m/s and temperature of 295 K. The equivalence ratio is maintained constant for all swirl numbers and equal to 0.83. The parameters of boundary and the operational conditions are enlisted in Table-1. The swirling action of flow is given to the airstream only. Swirling causes the flame to be widespread within the combustion chamber, and improves the combustion. In the present study, the dimensionless parameter as swirl number (S) shown in equation (1) is calculated as;

$$S = \frac{2}{3} \left(\frac{v_t}{v_a} \right) \left[\frac{1 - \left(\frac{r_i}{r_o} \right)^3}{1 - \left(\frac{r_i}{r_o} \right)^2} \right] \tan \beta \quad (1)$$

Swirl number is the ratio of the tangential and axial momentum fluxes. In the above equation, v_t and v_a represent the tangential and the axial components of the velocity of airflow, while r_i and r_o represent the internal and external swirl generator radius. In addition, β represent the angle of the swirlervane[22].

Table 1. Operational conditions of Harwell combustor.

Geometry:

Fuel inlet zone (mm)	$r_i=0.0$,	$r_o= 6.0$
Air inlet zone (mm)	$r_i=16.5$,	$r_o= 27.5$
Furnace radius (mm)	150	
Furnace length (mm)	900	
Inlet boundary conditions for fuel and air:	Fuel (m/s)	Air (m/s)
Axial velocity	15	12.8
Radial velocity	0	0
Swirl no.	0	0.4
Turbulent kinetic energy (m^2/s^2)	2.26	1.63
Turbulent dissipation rate (m^2/s^3)	1131.8	692
Temperature	295	
Composition (mass fraction) Fuel Air:	Fuel	Air
Oxygen	0	0.2315
Nitrogen	0	0.7685
Methane	1	0

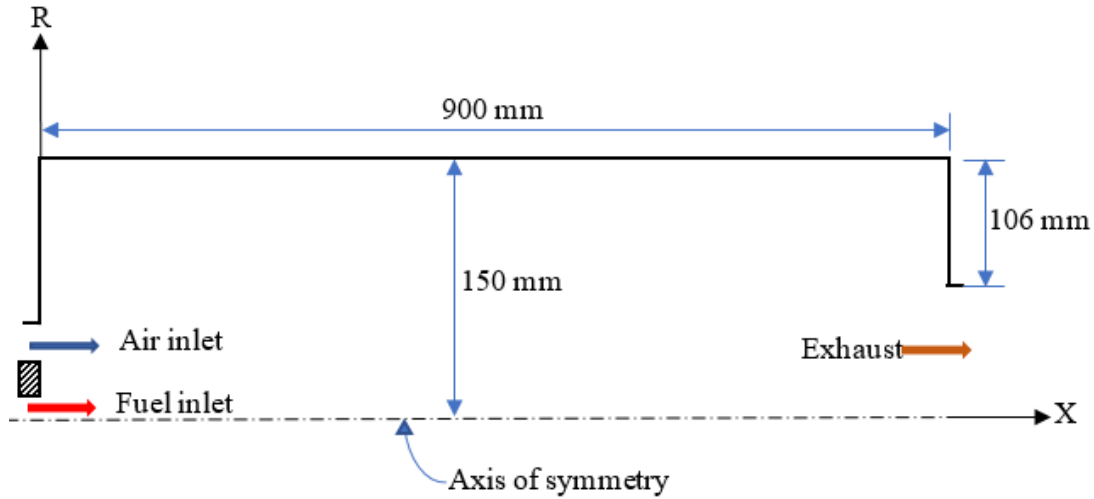


Figure 1. Combustion chamber geometry

2.2. Mathematical modeling

In the present study, a two-dimensional axisymmetric geometry is prepared, and the governing equations for the polar coordinate system are discretized with the help of the finite volume discretization method. Ansys Fluent 19.2 is used for simulation. The universal forms of Reynolds averaged governing equations are expressed as follows:

Continuity equation

$$\frac{\partial}{\partial x_i} \rho \bar{u}_i = 0 \quad (2)$$

Where, ρ represents the gas density and \bar{u}_i is the time average flow velocity vector.

Momentum conservation equation

$$\frac{\partial}{\partial x_i} (\rho \bar{u}_i \bar{u}_j) = \frac{\partial \bar{p}}{\partial x_i} + \frac{\partial}{\partial x_j} (\bar{\tau}_{ij} - \rho \overline{u'_i u'_j}) \quad (3)$$

Where \bar{p} is the time average mean static pressure, $\bar{\tau}_{ij}$ is the stress tensor expressed as

$\bar{\tau}_{ij} = \left[\mu \left(\frac{\partial \bar{u}_i}{\partial x_j} + \frac{\partial \bar{u}_j}{\partial x_i} \right) \right]$ and $-\rho \overline{u'_i u'_j}$ is the time-averaged Reynold's stress.

Energy conservation equation

$$\frac{\partial}{\partial x_i} (\rho \bar{u}_j \bar{h}) = \frac{\partial}{\partial x_i} \left(\frac{\mu}{\sigma} \frac{\partial \bar{h}}{\partial x_i} - \rho \overline{h' u'_i} \right) + S_{rad} + S_E \quad (4)$$

Where $\rho \overline{h' u'_i} = \left(\frac{\mu_t}{\sigma_{ht}} \frac{\partial \bar{h}}{\partial x_i} \right)$ is the turbulent flux for enthalpy. Here μ_t is the turbulent viscosity and σ_{ht} is the turbulent Prandtl number. S_{rad} is the radiative source term and S_E is the combustion reaction heat generation term.

Species mass conservation equation

$$\frac{\partial}{\partial x_i} (\rho \bar{u}_j \bar{Y}_k) = \frac{\partial}{\partial x_i} \left(\frac{\mu}{Sc} \frac{\partial \bar{Y}_k}{\partial x_i} - \rho \overline{Y'_k u'_i} \right) + \dot{\omega}_k \quad (5)$$

where, $\rho \overline{Y'_k u'_i} = \left(\frac{\mu_t}{Sc_t} \frac{\partial \bar{Y}_k}{\partial x_i} \right)$ is the turbulent flux for species. Here Sc_t is the turbulent Schmidt number and $\dot{\omega}_k$ represents the net rate of production of species in the species conservation equation. Reynolds stresses and all other turbulent fluxes are evaluated with the help of the Boussinesq hypothesis. k- ϵ turbulent model [23] is used to evaluate the turbulent quantities inflow field.

2.3. Radiation Model

Radiation is an important phenomenon in hydrocarbon fuel combustion as the products such as; H₂O and CO₂ diligently participate in radiation heat transfer. Moreover, due to the higher emissivity of soot, soot formation enhances the radiation heat loss [16]. DO model [16] can

calculate the effect of participating media and soot in radiation. The radiation transport equation (RTE) is expressed as;

$$\frac{dI(\vec{r}, \vec{s})}{ds} = \kappa I_b(\vec{r}) - \kappa I(\vec{r}, \vec{s}) \quad (6)$$

In the above equation, I is the radiation intensity, I_b is the black body radiation intensity, \vec{r} and \vec{s} are the position vector and direction vector respectively. κ is the bulk gas absorptivity including absorption coefficient of soot ($\kappa = \kappa_{gas} + \kappa_{soot}$).

Weighted sum grey gas model (WSSGM) model is used to evaluate absorptivity of bulk gas is expressed as;

$$\kappa_{gas} = - \frac{\ln \left[1 - \sum_{k=0}^{k=1} a_k (1 - e^{-\kappa_k p_k}) \right]}{z} \quad (7)$$

In the above equation, κ_k is the gray gas absorption coefficient for k^{th} participating gray gas. z is the path length which depends upon mesh size, p_k is the partial pressure of k^{th} gray gas, (a_k) is the emissivity weighing factor for k^{th} gray gas. It is a polynomial function of temperature which is expressed as;

$$a_k = \sum b_{k,j} T^j \quad (8)$$

The absorption coefficient of soot which is contributed to overall absorptivity is expressed as;

$$\kappa_{soot} = 1232.4 \rho_{soot} [1 + 4.8 \times 10^{-4} (T - 2000)] \quad (9)$$

The source term in the energy equation due to radiation which is described as the divergence of radiative heat flux $q(\vec{r})$ is expressed as;

$$\dot{S}_{rad} = \nabla \cdot q(\vec{r}) = \kappa \left[4\pi \frac{\sigma T_g^4}{\pi} - \int_0^{4\pi} I(\vec{r}, \vec{s}) d\Omega \right] \quad (10)$$

In the above equation, Ω is the solid angle.

2.4. Soot model

Hydrocarbon fuel produces soot during combustion at high temperatures. Soot is formed through four stages, such as nucleation, coagulation of hydrocarbons, surface growth, and soot also depletes through oxidation [24]. The nucleation and oxidation rate of soot are relatively slow as compared to the combustion process. Therefore, it requires different transport equations to solve the soot mass concentration and soot density in the computational domain [25]. Moss and Brookes [26], is an appropriate model to predict soot in a methane-air diffusion flame. This model has two soot transport equations. One is to find the number density and another is to find the mass concentration of the soot. The source term for number density can be written as

$$\frac{dN}{dt} = \underbrace{C_\alpha N_A \left(\frac{X_{C_2H_2} P}{RT} \right) \exp\left(-\frac{T_\alpha}{T}\right)}_{\text{Nucleation}} - \underbrace{C_\beta \left(\frac{24 RT}{\rho_{soot} N_A} \right)^{1/2} d_{soot}^{1/2} N^2}_{\text{Coagulation}} \quad (11)$$

and the source term for soot mass fraction can be expressed as;

$$\frac{dM}{dt} = \underbrace{C_\alpha M_p \left(\frac{X_{C_2H_2} P}{RT} \right) \exp\left(-\frac{T_\alpha}{T}\right)}_{\text{Nucleation}} + \underbrace{C_\gamma \left(\frac{X_{C_2H_2} P}{RT} \right) \exp\left(-\frac{T_\gamma}{T}\right) \left[(\pi N)^{\frac{1}{3}} \left(\frac{6M}{\rho_{soot}} \right)^{\frac{2}{3}} \right]^n}_{\text{Surface Growth}} - \underbrace{C_{oxid} C_\omega \eta_{coll} \left(\frac{X_{OH} P}{RT} \right) \sqrt{T} (\pi N)^{\frac{1}{3}} \left(\frac{6M}{\rho_{soot}} \right)^{\frac{2}{3}}}_{\text{Oxidation}} \quad (12)$$

It can be observed that the entire source term equation is a function of pressure, temperature, the universal gas constant, and mole fraction of precursor species C_2H_2 in nucleation and surface growth term and mole fraction of OH in oxidation term. Since the single-step global methane reaction mechanism is used in this work, the precursor species C_2H_2 species is absent in the chemistry. Therefore, to determine the soot precursor C_2H_2 within the computational domain, a relation between the mole fraction of C_2H_2 and mixture fraction ξ has been used. It is given as [27];

$$0 < \xi \leq 0.0575$$

$$X_{C_2H_2} = 5.277237 \times 10^{-2} \xi^2 - 1.920161 \times 10^{-5} \xi + 3.797003 \times 10^{-6} \quad (13)$$

$$0.0575 < \xi \leq 0.128$$

$$X_{C_2H_2} = 1599627 \xi^6 - 932192 \xi^5 + 223543.4 \xi^6 - 28182.59 \xi^3 + 1964.038 \xi^2 - 71.3474 \xi + 1.0513 \quad (14)$$

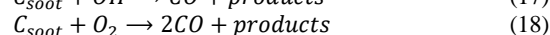
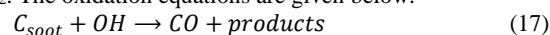
$$0.128 < \xi \leq 1$$

$$X_{C_2H_2} = 4.273195 \times 10^{-4} \xi^2 - 8.440912 \times 10^{-3} \xi + 7.988928 \times 10^{-3} \quad (15)$$

In the above equations ξ is mixture fraction inside the computational domain is expressed as;

$$\xi = \frac{\bar{Y}_{fu}}{\bar{Y}_{fu} + \bar{Y}_{ox}} \quad (16)$$

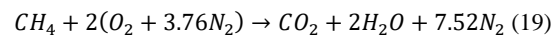
where, \bar{Y}_{fu} is the mass fraction of fuel and \bar{Y}_{ox} is the mass fraction of oxidizer (air) inside the computational domain. When $\xi = 1$, there is only fuel and no other species and for $\xi = 0$, there is an only oxidizer and no other species. The various constants used in equations 8 and 9 are taken from [27]. The turbulence effect on soot production or oxidation has been obtained through coupling with time-averaged temperature/species within the computational domain. A partial equilibrium oxidation model proposed by Fenimore-jones [27] is used to simulate soot oxidation. In the oxidation process, soot is oxidized with OH radical for methane fuel and partly with O_2 . The oxidation equations are given below.



However, in this model, only OH radical is considered for soot oxidation. The reaction rate is determined by the last term of the soot mass fraction source term.

2.5. Numerical Modeling

In the current investigation, the commercial ANSYSFluent 19.2 [28] has been used for computational analysis. The combustor geometry is prepared by following the work of Wilkies et al. [15]. SIMPLE algorithm is used for the coupling of pressure and velocity. All equations are solved with a second-order upwind scheme. The convergence residual value is kept as 10^{-6} for the energy equation, whereas it is set to 10^{-4} for all other governing equations. The standard k- ϵ model has been selected for turbulent flow modeling in the present work. The Eddy dissipation combustion model [29] is used for turbulent chemistry interaction. One step global reaction mechanism has been used for the combustion of methane-air.



DO radiation model is used in this study. This model has the potential to consider the radiation heat exchange between the gaseous phase and the soot present in the flame [30]. However, the P-1 and DO radiation model predicts equally. Habibi et al. [31] compared the prediction performance of the P-1 and DO radiation model on flame and reported that both models predict equally. Moreover, by using the weighted-sum-of-gray-gases model (WSGGM) [32], the absorption coefficient of the radiation is evaluated.

The thermophysical properties of all species used for the simulations are taken from the Fluent database, which is well verified. The specific heat for the mixed gas is evaluated as the mass-weighted averaging method. Moreover, it is taken as the polynomial function of temperature. The density of mixed gas is evaluated following incompressible ideal gas law. However, the conductivity is taken as constant because it does not vary significantly with temperature. The approximate dilution method is used for mass diffusion, where a constant diffusivity between all gases and the mixture is used. The viscosity of individual gas and the mixture gas is also taken as a polynomial function of temperature.

3. Grid Independence and model validation

3.1. Grid independency test and model validation

To reduce the computational cost and enhance the accuracy, the grid independence test has been performed. To investigate the mesh size effect, the test has been conducted for four different mesh sizes including 12,245, 34,542, 67,050 and 1,21,545 nodes before the actual numerical simulations start. The comparison has been done based on the axial temperature distribution inside the combustion chamber. The numerical results were compared with experimental results by Wilkies et al. [15] to determine the optimum mesh size for the numerical simulations. According to figure-2 (a), the mesh sizes of 67050 nodes and 121545 nodes are very much compatible with the experimental data and there is not much significant difference between the results with nodes 67050 and 121545. However, the grid with 67050 nodes is chosen for simulation to obtain fair results in the minimum possible time.

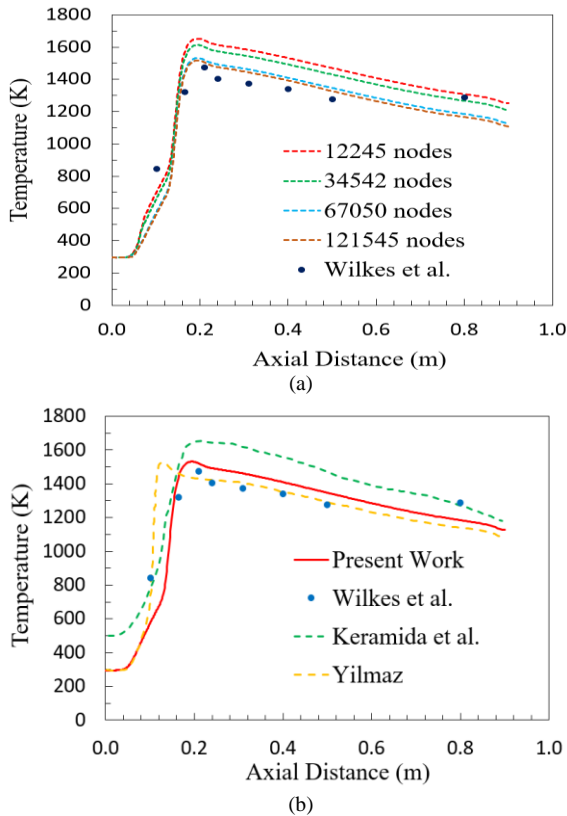


Figure 2. (a) The comparison for grid independence and (b) Numerical result validation: Yilmaz et al. [18]

The figure-2 (b) represents the axial temperature distributions. The predicted axial temperature has a good agreement with the experimental data of Wilkes et al.[15]. Moreover, the overall prediction of the current simulation is somehow better as compared to Keramida et al.[14] and Yilmaz [18].

4. Result and discussion

The effect of swirl intensity on flow behavior is illustrated through streamlines in figure-3. In the present study, the simulations are performed with swirl numbers 0.0, 0.1, 0.2, 0.3, 0.4, 0.5 and 0.6. Irrespective of swirl number a corner recirculation zone (CRZ) is formed due to the sudden expansion of air and fuel into the combustion

chamber. From the figure, it is observed that, with no swirl(SN= 0.0), the re-attachment length becomes maximum. With a further increase in the swirl intensity, the reattachment length for the CRZ decreases due to an increase in the radial component of the flow variable. When the swirl number is increased to 0.4, a central toroidal recirculation zone (CTRZ) is formed closer to the inlet of the combustion chamber. The formation of CTRZ is caused by a stronger swirl. Due to the formation of CTRZ, an adverse pressure gradient pulls the flame back. Hence, the flame becomes stable with increased swirl number, and the possibility of the flame blow out decreases.

Figure-4 (a) illustrates the axial temperature distribution on the symmetry axis for different swirl numbers. It can be seen that the maximum flame temperature location is shifted towards the inlet of the combustion chamber as we increase the intensity of the swirl. It is also observed that with the increase in swirl intensity, the maximum temperature on the axis of symmetry decreases. When the swirl number is higher than 0.3, a stronger CTRZ forms, hence the flame breaks as shown in figure 5. As a result, the highest flame temperature with these higher swirl numbers does not fall on the axis, rather shifts towards the wall region. For no swirl, the flame temperature is higher as compared to swirled flow, and the peak is observed at the farthest position from the inlet region because the flame is not pulled back due to the absence of an adverse pressure gradient. With the increase in swirl intensity, the flame length decreases, and flame width increases due to the presence of an adverse pressure gradient. Figure-4 (b) illustrates the radial distribution of temperature along the radial direction at the exit of the combustor. It is observed that, with strong swirls (swirl number greater than 0.3), the temperature distribution across the exit plane is uniform, which can also be observed in figure 5. It happens due to the CTRZ formation, which widens the flame and protects the flame from stretching. On the other hand, elongated flame produces a non-uniform temperature distribution across the exit plane due to weak swirl or no swirl. Also, the axial temperature at the exit is high.

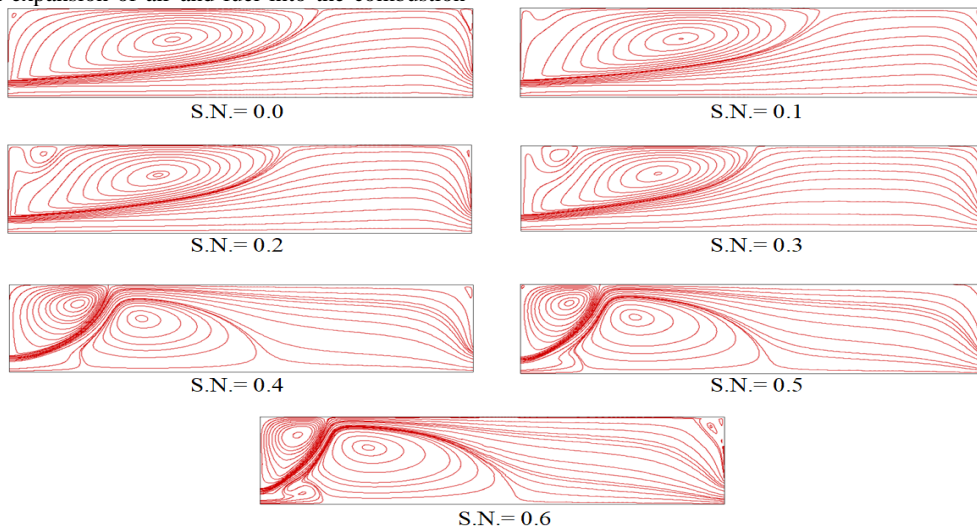


Figure 3. Streamlines flow for different swirl numbers.

The widening of flame and flame breakdown due to high swirling action causes heat loss from the flame through the combustor wall. The peak flame temperature region becomes closer to the combustor wall due to swirling action. As a result, the radiative heat losses increase. However, the lower flame temperature due to

higher swirling action decreases the formation rate of thermal NO_x. This is an advantage of swirling as well. Moreover, the uniformly distributed temperature is very much needed in the case of heating and baking furnaces to improve the quality of the product.

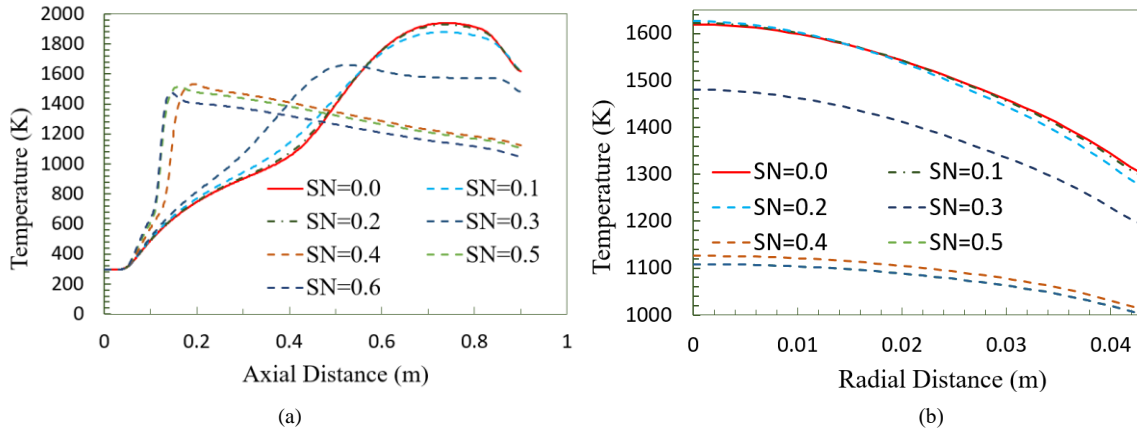


Figure 4. Variation of (a) axial temperature and (b) exhaust temperature with different swirl numbers.

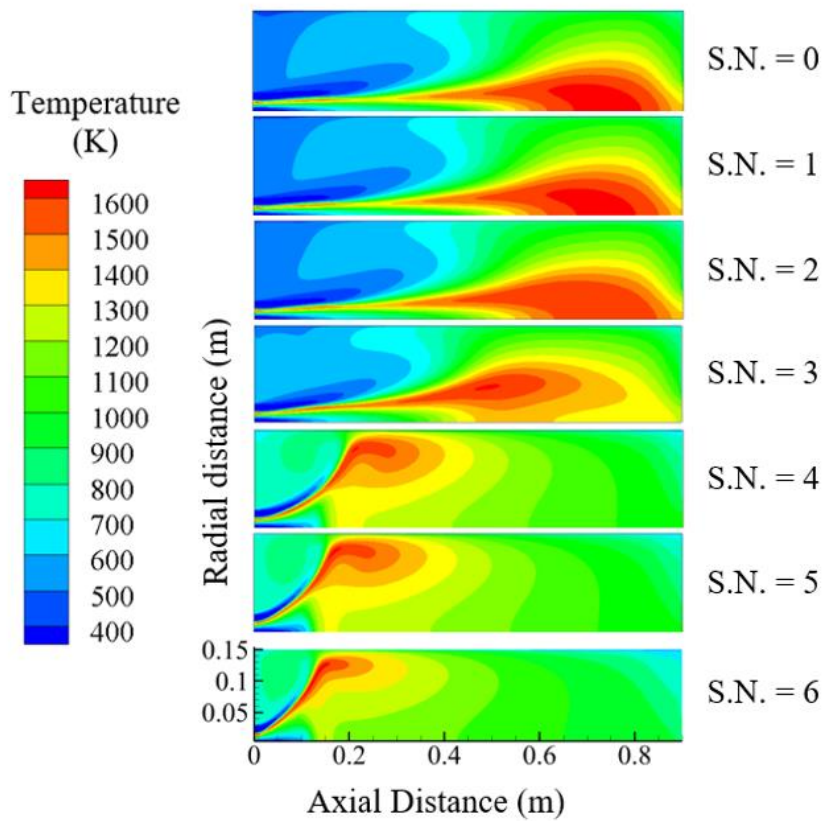


Figure 5. Temperature distribution contours for different swirl numbers.

Figure-6 (a) illustrates the effect of swirl intensity on radiation heat flux along the combustor wall. From the diagram, it is clear that the swirl intensity strongly affects the radiative heat transfer along the combustor wall. It has been observed that, for a strong swirl (swirl number greater than 0.3), the maximum wall radiative heat flux is observed at a little ahead of the inlet region. This wall heat flux depends on the flame position and flame temperature. Figure 5 reveals that, for a stronger swirl, the high-temperature zone of flame is closer to the wall and also is closer to the inlet. As swirl strength decreases, the flame becomes stretched and a high-temperature zone of the flame exists at the downstream region. Thus higher radiative heat transfer occurs from the flame to the combustor wall at the downstream region. Figure-6(b) shows the area-weighted average heat flux at the combustor wall for different swirl numbers. The temperature field near the entire combustor wall is very high with a higher swirl number. As a result average wall heat flux is higher for higher swirl number cases.

Figure 7 illustrates the soot volume fraction along the axis at different inlet swirls. Soot formation rate is directly related to the local equivalence ratio within the reaction zone. Soot formation rate becomes higher within the reaction zone, where the air-fuel mixture is relatively richer. Figure 9a. and 9b. (SN=0 and 0.3), clearly show a significant fuel mass fraction throughout the length of the combustor along the axis. It indicates that in this region relatively richer mixture causes the formation of a higher

amount of soot. As a result, for low inlet swirls (SN=0.0 to 0.3), a relatively higher soot volume fraction is observed along the entire length of the flame on the axis of symmetry as shown in figure 7. On the other hand, for a higher swirl (SN=0.4 to 0.6), significant fuel concentration is observed up to 0.15 m from the inlet as shown in figure 9c (for SN=0.6). Therefore, a higher amount of soot is observed in this region for higher inlet swirl cases. Beyond this region, soot volume fraction significantly decreases up to the exit of the combustor due to the absence of a rich mixture.

From figure-5, it has been observed that the flame structures are pretty similar for the SN 0.0, 0.1, and 0.2. Similarly, the flame structures are pretty similar for SN 0.4, 0.5, and 0.6. However, with SN 0.3, the flame structure is different than others; hence it is a transition kind of structure, where the flame is neither too stretched nor too short. It is well known that soot mass concentration is a strong function of temperature along with precursor species concentration. From the equations 13-15, if a graph will be drawn for $X_{C_2H_2}$ Vs ξ , it can be noticed that for the value of $\xi=0.15$, $X_{C_2H_2}$ is maximum. Most probably for the SN=0.3, the value of ξ is closer to 0.15 in most of the regions. However, the value of ξ depends upon the mixing of fuel and oxidizer. Here probably the mixing of fuel and oxidizer is much better than other swirl number cases. This may be the reason for the difference in soot volume fraction distribution for SN = 0.3.

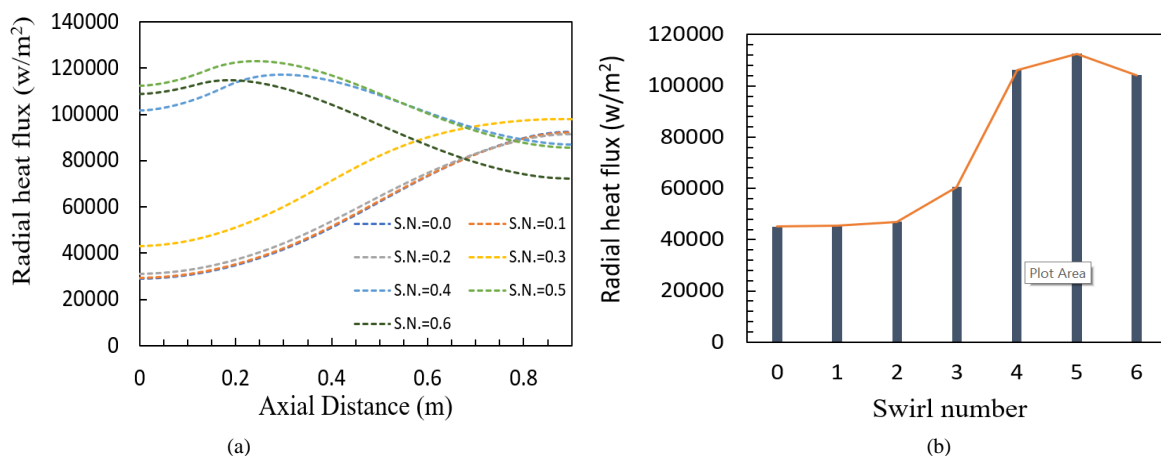


Figure 6. (a)Variation of radiation heat flux at the wall with different swirl numbers and (b) Average of radiation heat flux at the wall with different swirl numbers

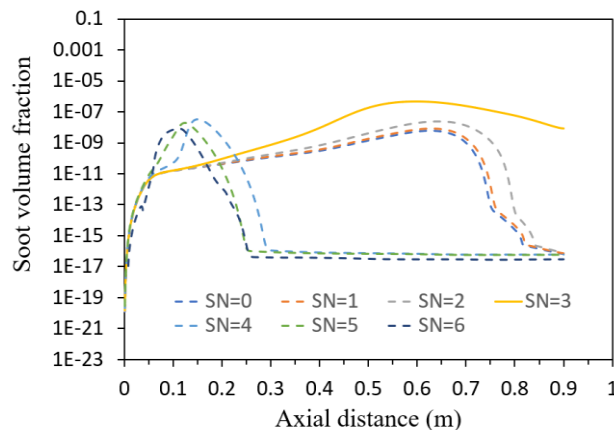


Figure 7. Soot volume fraction along the axis at different inlet swirl

Figure-8 shows the effect of soot on wall radiation heat flux at different swirl strengths. The comparison is made for non-swirling state (swirl number = 0.0) and swirl numbers 0.3 and 0.6. From the diagram, it is clear that the formation of soot enhances the radiation heat transfer irrespective of inlet swirl intensity. Soot is a black body, hence a considerable amount of heat is emitted when soot presents in flame. As a result flame temperature decreases and wall heat flux increases, when soot presents in flame. However, maximum wall heat flux differences are observed in between the conditions; flame with soot and flame without soot at a particular position along the wall length. This maximum difference position can be identified by comparing figure 7 and figure 8 simultaneously. It is obvious that where the soot concentration is the highest, the wall radiative heat flux difference becomes highest at this location along the combustor length.

Figure-9 illustrates the major species (CH_4 , O_2 , CO_2 , and N_2) mass fraction along the axis of symmetry for a non-swirling state ($\text{SN} = 0.0$), swirl number 0.3, and swirl number 0.6. Since the fuel stream is aligned with the axis of symmetry, therefore at the inlet, there is only fuel. Hence, here (at $x = 0$ m) mass fraction of fuel is 1

irrespective of the swirl number. After a certain distance (around $x = 0.05$ m), fuel concentration decreases and CO_2 formation starts. It confirms that the reaction zone starts from here along the axis. When there is no swirl or very low swirl intensity, the fuel is consumed completely far away from the inlet along the axis. This is due to stretched flame and thicker reaction zone. On the other hand, when the swirl intensity is 0.6, fuel is consumed completely closer to the inlet along the axis. This is due to the short flame and thinner reaction zone. However, it is observed that, when the swirl number is 0.6, beyond the reaction zone, the products are well diffused. As a result, no variations of species are observed along the axis, beyond the reaction zone. comparing the species mass fraction graph with the temperature distribution contours, figure-5, it is found that the peak for CO_2 mass fraction and zero fuel concentration is observed with the location of maximum temperature in the combustion chamber. When swirl intensity is increased, this point on the symmetry axis comes closer to the inlet of the furnace. Similarly, the mass fraction of other species (O_2 , N_2) also reach their peak values at the location of maximum temperature. This represents the occurrence of the true combustion process.

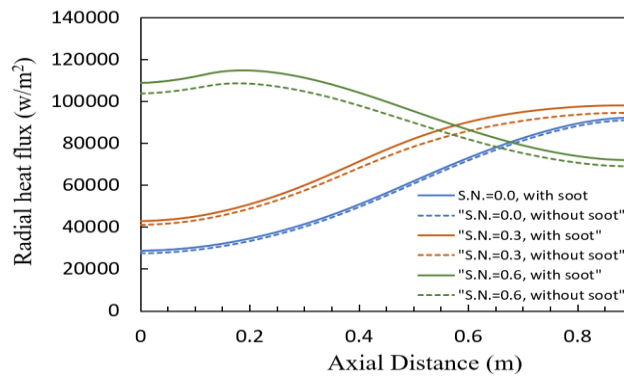


Figure 8. Variation of radiation heat flux at the wall with and without soot at different swirl numbers

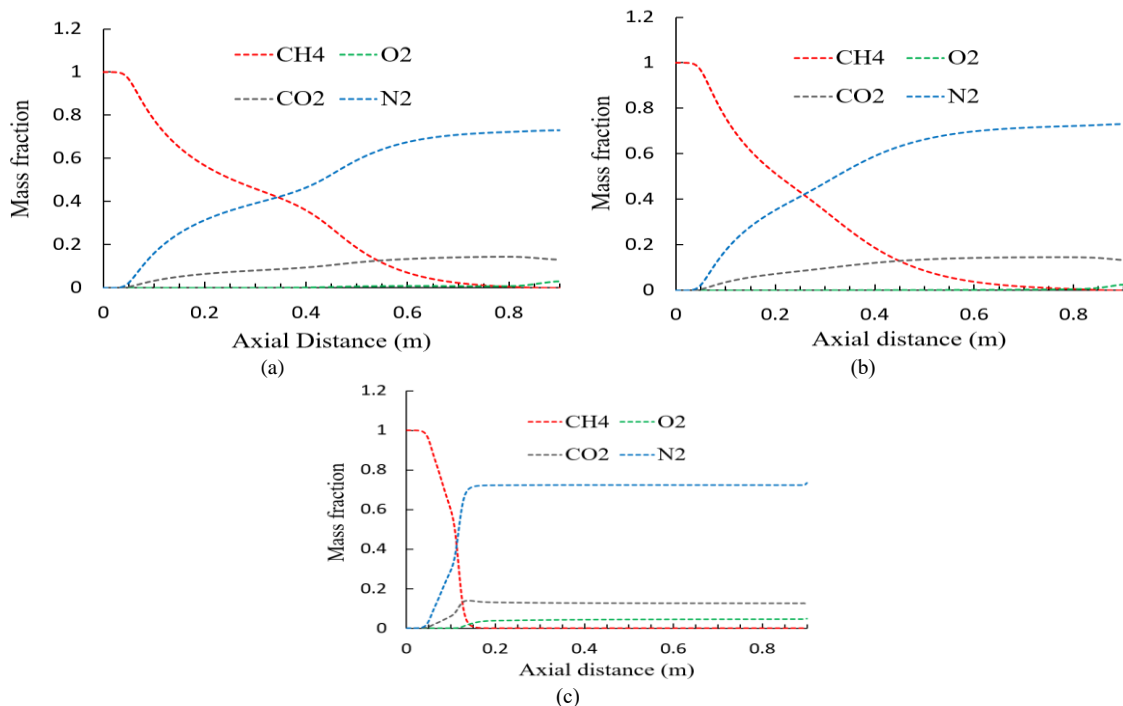


Figure 9. Species mass fraction on axis of symmetry for different swirl numbers. (a) Swirl number = 0.0, (b) Swirl number = 0.3 and (c) Swirl number = 0.6

5. Conclusion

In the present study, numerical simulations have been performed on the Harwell furnace model to assess the effect of swirl intensity on combustion characteristics, such as dynamic flow behavior, temperature distribution contours, heat transfer flux at furnace wall, soot formation, and species mass fraction distribution. The main conclusions are summarized as follows.

- A central toroidal circulation zone forms closer to the inlet of the air-fuel region as the swirl number increases beyond 0.3, and thereby a better air-fuel mixture is prepared. Moreover, the central circulation zone enhances the backflow movement in the flow field and thus the residence time for the fuel inside the combustion zone is increased. This results in an incomplete combustion of fuel and hence the possibility of pollutant formation becomes minimum.
- With increasing swirl intensity, it is found that the fluid flow pattern is widened radially in the combustion chamber and the temperature distribution throughout the furnace is uniformly distributed. Particularly at the outlet, the temperature distribution becomes more uniform and lower. As a result, the possibility of formation thermal NO_x becomes minimum.
- The soot formation is 45.65% higher, at the exit when the swirl number is greater than 0.3 as compared to the no swirl case.
- The radiant heat transfer flux increases as the swirl intensity increases. When the swirl number is more than 0.3, the heat transmission rate nearly doubles. It is consistently distributed along the furnace wall. The heat transfer rate is further enhanced by eight percent with the formation of soot in the fuel-rich region of the flame. As compared to no swirl, the average wall heat flux increases to 62.72% when the swirl number is 5.
- During combustion, the fuel mass fraction is properly utilized and its distribution along the centerline of the furnace becomes uniform with the rise of the swirl intensity.

References

- [1] K. Schofield, *Combustion emissions: Formation, reaction, and removal of trace metals in combustion products*. Elsevier, 2020.
- [2] L. X. Zhou, X. L. Chen, and J. Zhang, "Studies on the effect of swirl on NO formation in methane/air turbulent combustion," *Proc. Combust. Inst.*, vol. 29, no. 2, pp. 2235–2242, 2002, doi: 10.1016/s1540-7489(02)80272-3.
- [3] N. Merlo et al., "Combustion characteristics of methane-oxygen enhanced air turbulent non-premixed swirling flames," *Exp. Therm. Fluid Sci.*, vol. 56, pp. 53–60, 2014, doi: 10.1016/j.expthermflusci.2013.11.019.
- [4] N. Syred and J. M. Beér, "Combustion in swirling flows: A review," *Combust. Flame*, vol. 23, no. 2, pp. 143–201, 1974, doi: 10.1016/0010-2180(74)90057-1.
- [5] C. O. Iyogun, M. Birouk, and J. A. Kozinski, "Experimental investigation of the effect of fuel nozzle geometry on the stability of a swirling non-premixed methane flame," *Fuel*, vol. 90, no. 4, pp. 1416–1423, 2011, doi: 10.1016/j.fuel.2010.12.033.
- [6] M. Saediamiri, M. Birouk, and J. A. Kozinski, "On the stability of a turbulent non-premixed biogas flame: Effect of low swirl strength," *Combust. Flame*, vol. 161, no. 5, pp. 1326–1336, 2014, doi: 10.1016/j.combustflame.2013.11.002.
- [7] D. Sellan and S. Balusamy, "Experimental study of swirl-stabilized turbulent premixed and stratified LPG/air flames using optical diagnostics," *Exp. Therm. Fluid Sci.*, vol. 121, no. August 2020, 2021, doi: 10.1016/j.expthermflusci.2020.110281.
- [8] S. Yoon, S. Lee, H. Kwon, J. Lee, and S. Park, "Effects of the swirl ratio and injector hole number on the combustion and emission characteristics of a light duty diesel engine," *Appl. Therm. Eng.*, vol. 142, no. June, pp. 68–78, 2018, doi: 10.1016/j.applthermaleng.2018.06.076.
- [9] H. Ogawa, Y. Matsui, S. Kimura, and J. Kawashima, "Three-dimensional computation of the effects of the swirl ratio in direct-injection diesel engines on NO_x and soot emissions," *SAE Tech. Pap.*, no. 412, 1996, doi: 10.4271/961125.
- [10] F. Bonatesta et al., "The Influence of Swirl Ratio on Soot Quantity and Distribution in the Cylinder of a Diesel Engine," *Third Eur. Combust. Meet. ECM*, no. November, pp. 1–6, 2007.
- [11] S. T. Chong, M. Hassanaly, H. Koo, M. E. Mueller, V. Raman, and K. P. Geigle, "Large eddy simulation of pressure and dilution-jet effects on soot formation in a model aircraft swirl combustor," *Combust. Flame*, vol. 192, pp. 452–472, 2018, doi: 10.1016/j.combustflame.2018.02.021.
- [12] H. Zhou, X. Li, and F. Liu, "Soot formation and oxidation mechanisms in a diesel engine separated swirl combustion system," *Fuel*, vol. 257, no. August, p. 115955, 2019, doi: 10.1016/j.fuel.2019.115955.
- [13] L. Y. Wang, S. Chatterjee, Q. An, A. M. Steinberg, and Ö. L. Gülder, "Soot formation and flame structure in swirl-stabilized turbulent non-premixed methane combustion," *Combust. Flame*, vol. 209, pp. 303–312, 2019, doi: 10.1016/j.combustflame.2019.07.033.
- [14] E. P. Keramida, H. H. Liakos, M. A. Founti, A. G. Boudouvis, and N. C. Markatos, "Radiative heat transfer in natural gas-fired furnaces," *Int. J. Heat Mass Transf.*, vol. 43, no. 10, pp. 1801–1809, 2000, doi: 10.1016/S0017-9310(99)00244-6.
- [15] S. Wilkes, N.S.; Guilbert, P.W.; Shepherd, C.M.; Simcox, "The application of Harwell-Flow 3D to combustion models," *At. Energy Auth. Report*, Harwell, UK, Pap. No. AERE-R-13508, pp. 1–17, 1989, [Online]. Available: <http://www.opengrey.eu/item/display/10068/630809>.
- [16] P. Ghose, J. Patra, A. Datta, and A. Mukhopadhyay, "Prediction of soot and thermal radiation in a model gas turbine combustor burning kerosene fuel spray at different swirl levels," *Combust. Theory Model.*, vol. 20, no. 3, pp. 457–485, 2016, doi: 10.1080/13647830.2016.1147607.
- [17] P. Ghose, A. Datta, R. Ganguly, A. Mukhopadhyay, and S. Sen, "Modelling of Soot Formation in a Kerosene Spray Flame," in *Modeling and Simulation of Turbulent Combustion*, Springer, Singapore, 2018, pp. 363–394.
- [18] İ. Yılmaz, "Effect of Swirl Number on Combustion Characteristics in a Natural Gas Diffusion Flame," *J. Energy Resour. Technol.*, vol. 135, no. 4, pp. 1–8, 2013, doi: 10.1115/1.4024222.
- [19] X. Yang, Z. He, Q. Niu, S. Dong, and H. Tan, "Numerical analysis of turbulence radiation interaction effect on radiative heat transfer in a swirling oxyfuel furnace," *Int. J. Heat Mass Transf.*, vol. 141, pp. 1227–1237, 2019, doi: 10.1016/j.ijheatmasstransfer.2019.07.060.
- [20] L. K. Moey, M. F. Kong, V. C. Tai, T. F. Go, and N. M. Adam, "Effect of Gable Roof Angle on Natural Ventilation for an Isolated Building," *Jordan J. Mech. Ind. Eng.*, vol. 15, no. 3, pp. 291–300, 2021.
- [21] C. Ghenai, T. Salameh, and I. Janajreh, "Modeling and simulation of shrouded Horizontal Axis Wind Turbine using

- RANS method,” *Jordan J. Mech. Ind. Eng.*, vol. 11, no. Specialissue, pp. 235–243, 2017.
- [22] Ø. Spangelo, “Experimental and Theoretical Studies of a Low NO_x Swirl Burner,” *The Norwegian University of Science and Technology*, 2004.
- [23] A. J. Lew, G. C. Buscaglia, and P. M. Carrica, “A Note on the Numerical Treatment of the k-epsilon Turbulence Model,” *Int. J. Comput. Fluid Dyn.*, vol. 14, no. 3, pp. 201–209, 2001, doi: 10.1080/10618560108940724.
- [24] M. R. Busupally and A. De, “Numerical modeling of Soot formation in a turbulent C₂H₄/air diffusion flame,” *Int. J. Spray Combust. Dyn.*, vol. 8, no. 2, pp. 67–85, 2016, doi: 10.1177/1756827716638814.
- [25] I. M. Kennedy, “Models of soot formation and oxidation,” *Prog. Energy Combust. Sci.*, vol. 23, no. 2, pp. 95–132, Jan. 1997, doi: 10.1016/S0360-1285(97)00007-5.
- [26] S. J. Brookes and J. B. Moss, “Predictions of soot and thermal radiation properties in confined turbulent jet diffusion flames,” *Combust. Flame*, vol. 116, no. 4, pp. 486–503, 1999, doi: 10.1016/S0010-2180(98)00056-X.
- [27] C. P. Fenimore and G. W. Jones, “Soot by Hydroxyl Radicals,” *J. Phys. Chem.*, vol. 71, no. 3, pp. 593–597, 1967.
- [28] ANSYS Fluent User’s Guide Release 15.0. Canonsburg: ANSYS Incorporation, 2013.
- [29] B. F. Magnussen and B. H. Hjertager, “On mathematical modeling of turbulent combustion with special emphasis on soot formation and combustion,” *Symp. Combust.*, vol. 16, no. 1, pp. 719–729, 1977, doi: 10.1016/S0082-0784(77)80366-4.
- [30] R. Siegel and J. R. Howell., *Thermal Radiation Heat Transfer*. Washington DC: Hemisphere Publishing Corporation, 1992.
- [31] A. Habibi, B. Merci, and G. J. Heynderickx, “Multiscale Modeling of Turbulent Combustion and NO_x Emission in Steam Crackers,” *AIChE J.*, vol. 53, no. 9, pp. 2384–2398, 2007, doi: 10.1002/aic.11243.
- [32] M. F. Modest, “The weighted-sum-of-gray-gases model for arbitrary solution methods in radiative transfer,” *J. Heat Transfer*, vol. 113, no. 3, pp. 650–656, 1991, doi: 10.1115/1.2910614.